PNAS
www.pnas.org

Supplementary Information for

Directing the reactivity of metal hydrides for selective CO_2 reduction

Bianca M. Ceballos and Jenny Y. Yang

Jenny Y. Yang
Email: j.yang@uci.edu

This PDF file includes:

Supplementary text
Figs. S1 to S19
References for SI reference citations

www.pnas.org/cgi/doi/10.1073/pnas.1811396115

Supplementary Information Text

Synthetic Methods and Materials. All manipulations were carried out using standard Schlenk or glovebox techniques under an atmosphere of dinitrogen. Solvents were degassed by sparging with argon gas and dried by passage through columns of activated alumina or molecular sieves. Deuterated solvents were purchased from Cambridge Isotopes Laboratories, Inc. and were degassed and stored over activated 3 Å molecular sieves prior to use. Reagents were purchased from commercial vendors and used without further purification unless otherwise noted. Metal complex $[Pt(dmpe)_2](PF_6)_2$ (**3**) and $[HPt(dmpe)_2](PF_6)$ (**2**) were prepared and purified according to previously reported procedures.[1,2]

Physical Methods. ^1H and $^{31}P\{^1H\}$ nuclear magnetic resonance (NMR) spectra were collected at room temperature, unless otherwise noted, on a Bruker AVANCE 500 MHz spectrometer. Chemical shifts are reported in δ notation in parts per million (ppm). ^1H spectra referenced to residual proteo resonances of deutrated solvent. $^{31}P\ \{^1H\}$ spectra were referenced to H_3PO_4 at 0 ppm within Xwin-NMR or Bruker's Topspin software, which derives the chemical shifts from the known frequency ratios of the ^{31}P standard to the lock signal of the deuterated solvent. ^{31}P spectra used in determining concentration were obtained either with long delay times (20s) for 64 scans to ensure quantitative integration. Manual shimming, Fourier transformation, and automatic spectrum phasing were performed using Xwin-NMR software when using the 500 MHz spectrometer. Spectra were analyzed and figures were generated using MestReNova 6.0.2 software. Peak integrations were calculated within MestReNova.

Electrochemistry. Cyclic voltammetry was performed on a Pine Wavedriver 10 potentiostat with AfterMath software. For pre- and post-electrolysis solution analysis, CV was performed in the 150 mL glass controlled potential electrolysis cell using cylindrical carbon foam working and counter electrodes. All other CV experiments were performed in a 3 mL glass cell using glassy carbon working and counter electrodes. A glass jacketed silver wire reference electrode in 0.1 M $TBAPF_6$ acetonitrile solution separated from the bulk solution by a porous Vycor tip was used. Electrochemistry was performed on 0.5 mM or 1 mM solutions of analyte with appropriate amounts of phenol, 1 mM $Fe(C_5H_5)_2$, and 0.1 M $TBAPF_6$ as supporting electrolyte. For experiments carried out under CO_2, CO_2 gas was first run through a Drierite column and secondly through an acetonitrile bubbler. The acetonitrile-saturated CO_2 was used to sparge solution for at least 5 min before data collection, and the sample was kept under a blanket of CO_2 for the duration of the experiment.

Controlled Potential electrolysis and Product Analysis. Controlled potential electrolyses were performed in a Pine 150 mL cell with water jacket and five ground-glass ports (one 24/40, four 14/20). All cell ports were sealed with greased ground-glass joints with the exception of one 14/20 port, which was sealed with a SubaSeal rubber septum used for headspace sampling. Vitreous carbon foam rods were used for the working and counter electrodes, while a glass jacketed silver wire electrode in 0.1M $TBAPF_6$ fit with a Vycor tip was used as the reference. The carbon foam rods were attached to copper wire leads using conductive silver epoxy (AI Technology Prima-Solder EG8050) under Loctite epoxy. The counter electrode was separated from the bulk solution by a 10 mm glass tube with an extra-fine (Ace glass porosity E) fritted glass bottom; the tube was inserted through the 24/40 cell port and sealed with a ground-glass joint. The working and reference

electrodes were connected to the exterior of the cell via nickel sleeves joining the electrode leads to a tungsten wire that was sealed through a 14/20 ground-glass stopper. A mercury pool, contained in a shallow glass cup, was placed at the bottom of each electrolysis sample.

Cell headspace was sampled with a Restek A-2 Luer lock gas-tight syringe. Headspace hydrogen was quantified by gas chromatography on an Agilent 7890B instrument with a Molsieve column. GC method details are as follows: dinitrogen carrier gas, 40 °C column temperature, TCD detector at 220 °C; helium carrier gas, 40 °C column temperature, TCD detector at 220 °C. Calibration curve was generated by injecting known percentages of H_2 into the full electrolysis cell setup, including the appropriate amount of acetonitrile, and stirring for 1 hour (Figure S19). CO_2 gas was first run through a VICI Metronics CO_2 gas purification column and secondly through an acetonitrile bubbler to saturate CO_2 with acetonitrile vapor before sparging solution for 30 mins. The electrolysis cell sample was kept under a blanket of CO_2 for the duration of data collection and sealed under acetonitrile saturated CO_2.

The post-electrolysis solution was collected for solution product analysis, quantification and catalyst retention. $^{31}P\{^1H\}$ NMR was used to determine catalyst concentration before and after electrolysis, by comparing catalyst resonance integration area to that of the PF_6 anion in solution. The solution product formate was identified and quantified using ^1H NMR spectroscopy. Formate product concentration was determined by comparing resonance integration area to that of an added internal DMF standard.

Method A: A 0.5 mL sample of post-electrolysis solution with added DMF standard was diluted with 0.05 mL of CD_3CN and spectra were collected using 16 scans with long delay times (20 seconds).

Method B: Post-electrolysis solution was acidified using dilute HCl (0.1 M) and DMF aliquot was added. A sample of 0.5 mL of solution was diluted with 0.05 mL of CD_3CN and spectra were collected using solvent suppression, 16 scans and long delay times (20 seconds). Observed relative concentrations of formic acid to DMF standard were corrected using a calibration curve for formic acid in acetonitrile using solvent suppression ^1H NMR spectroscopy.

Observed rate constant (k_{obs}) calculation. An acid titration study was carried out on 0.5 mM solution of **3** at 10 mV/s scan rate with microliter additions of 1 M phenol in acetonitrile under CO_2. Acid was titrated to solution of **3** saturated with CO_2 resulting in catalytic current increase where max catalytic current (i_c) was observed after 10 equivalents of phenol.

The observed rate constant (k_{obs}) was calculated using the relationship between catalytic current (i_c) and peak current (i_p) in the absence of acid and CO_2 described in Eq. S3.[3,4] In Eq. S1 describing i_c, n is the number of moles consumed in a catalytic cycle, F is Faraday's constant, A is the electrode surface area, $[Cat]_T$ is catalyst concentration, D is the diffusion coefficient, and k_{obs} is observed rate constant. In contrast, in Eq. S2 describing i_p, n' is the number of electrons consumed by the catalyst, υ is scan rate, R is the ideal gas constant, and T is temperature. Solving the i_c-i_p relationship (Eq. S3) for k_{obs} results in an expression that is independent of D, A and $[Cat]_T$ (Eq. S4). This expression can be used to calculate k_{obs} in pure kinetic zones where S-shaped curves are observed and i_c is not limited by substrate diffusion.[5]

$$i_c = nFA[\text{Cat}]_T(Dk_{obs})^{1/2} \quad \text{Eq. S1}$$

$$i_p = 0.446n'FA[\text{Cat}]_T(D\upsilon)^{1/2}(n'F/RT)^{1/2} \quad \text{Eq. S2}$$

$$\left(\frac{i_c}{i_p}\right) = \frac{n(k_{obs})^{1/2}}{0.446n'(\upsilon)^{1/2}(n'F/RT)^{1/2}} \quad \text{Eq. S3}$$

$$k_{obs} = \left[\left(\frac{i_c}{i_p}\right)\frac{0.446}{n}\right]^2 (n')^3 F\frac{\upsilon}{RT} \quad \text{Eq. S4}$$

scan rate (V/s)	n	n'	*ic* (uA)	*ip* (uA)	*ic/ip*	k_{obs}
0.01	2	2	1.92	1.05	1.8	0.5

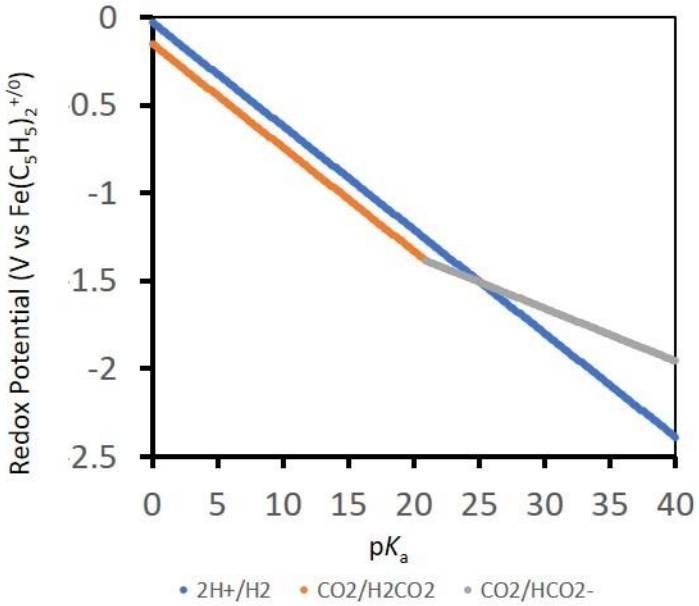

Fig. S1. Pourbaix diagram displaying the thermodynamic potentials for $2H^+/H_2$ (blue), CO_2/H_2CO_2 (orange) and CO_2/HCO_2^- (gray) in CH_3CN.

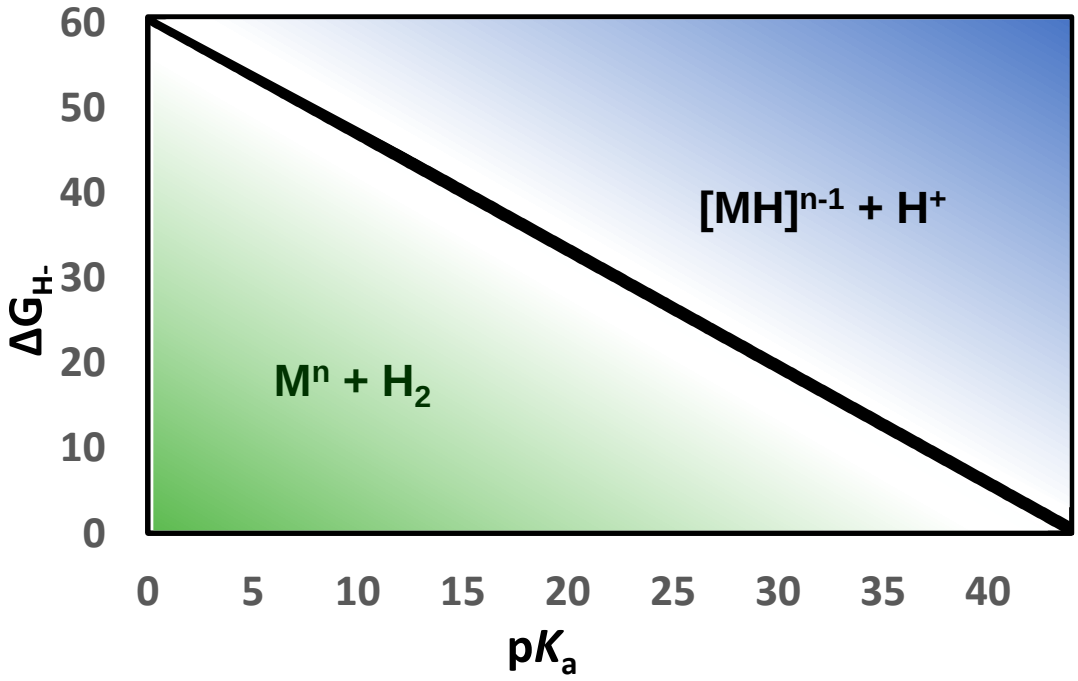

Fig. S2. Thermodynamic product diagram showing the relationship between hydricity (ΔG_{H^-}) and stability at various pK_a values to H_2 evolution in dimethylsulfoxide.

.

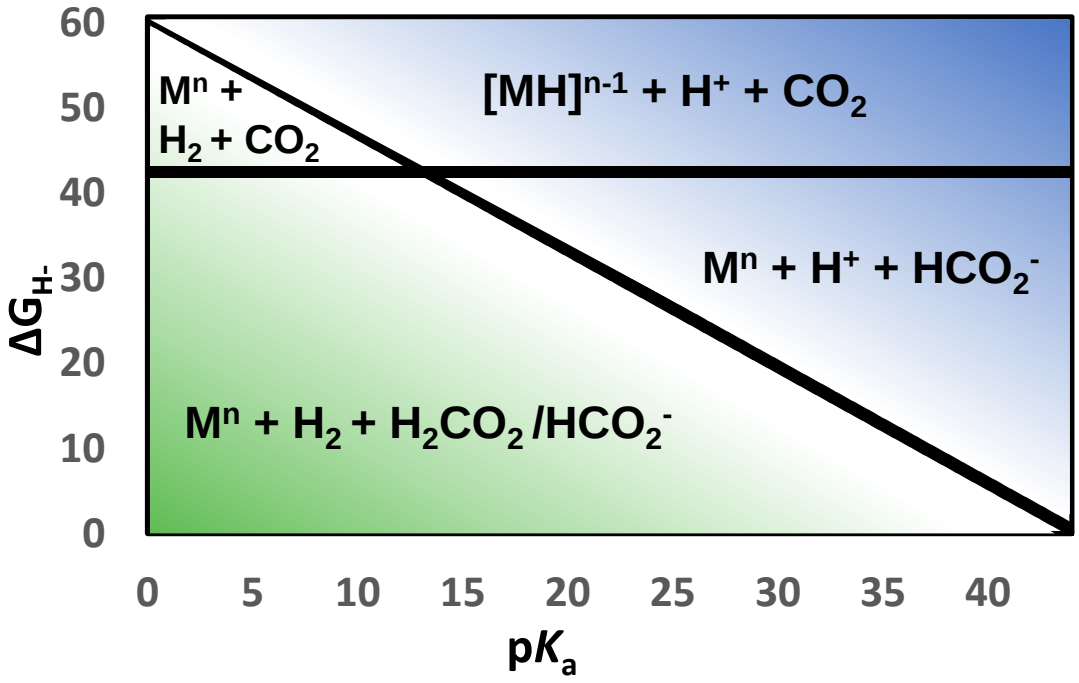

Fig S3. Thermodynamic product diagram showing the relationship between hydricity (ΔG_{H^-}) and reactivity towards H^+ of various pK_a values to H_2 evolution or CO_2 reduction in dimethylsulfoxide.

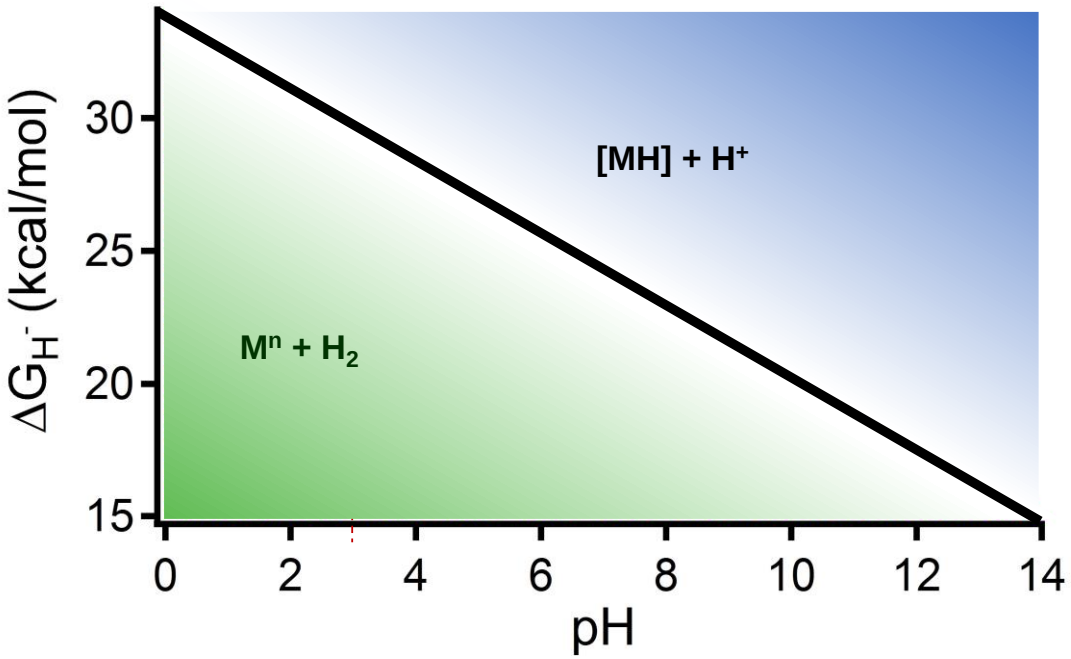

Fig. S4. Thermodynamic product diagram showing the relationship between hydricity (ΔG_{H^-}) and stability at various pH values to H_2 evolution in water.

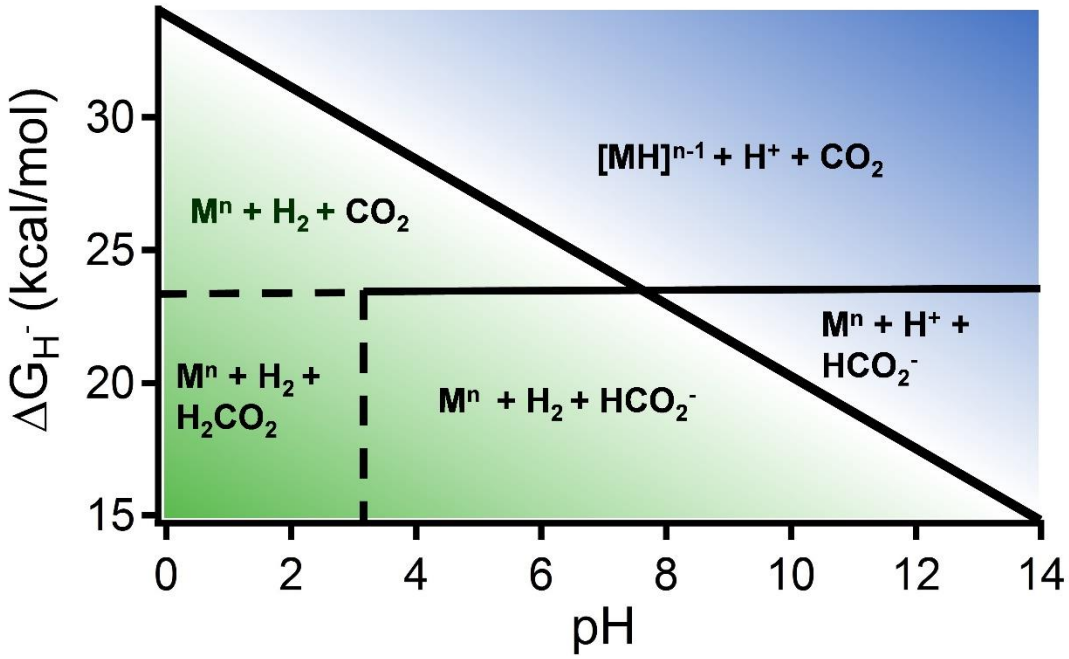

Fig. S5. Thermodynamic product diagram showing the relationship between hydricity (ΔG_{H-}) and reactivity towards H^+ of various pH values to H_2 evolution or CO_2 reduction in water.

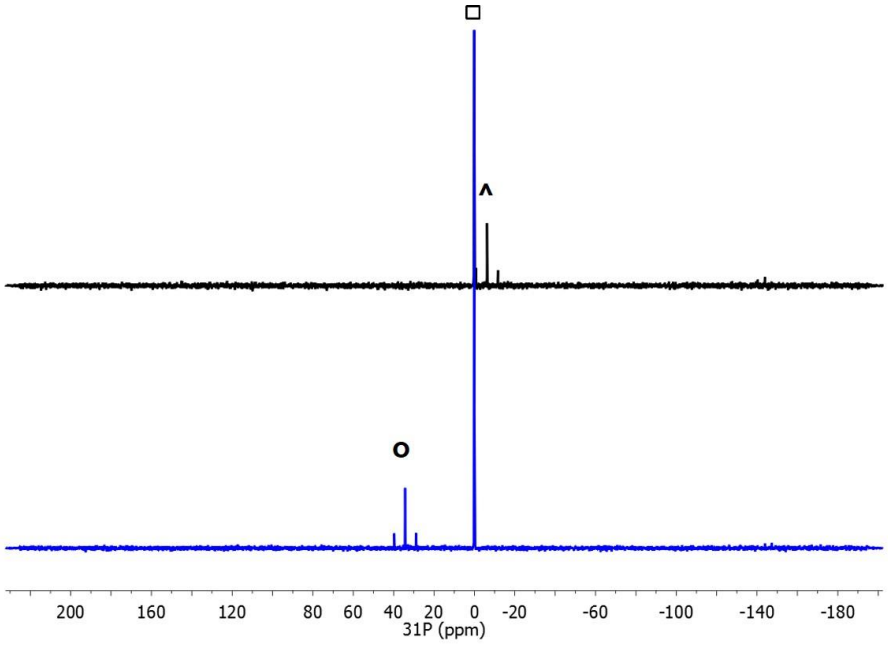

Fig S6. $^{31}P\{^{1}H\}$ NMR spectra of $[HPt(dmpe)_2](PF_6)$ (top) and after addition 1 equivalent of anilinium tetrafluoroborate (bottom). Where ^ denotes $[HPt(dmpe)_2]^+$, **o** denotes $[Pt(dmpe)_2]^{2+}$, and • denotes H_3PO_4 in capillary.

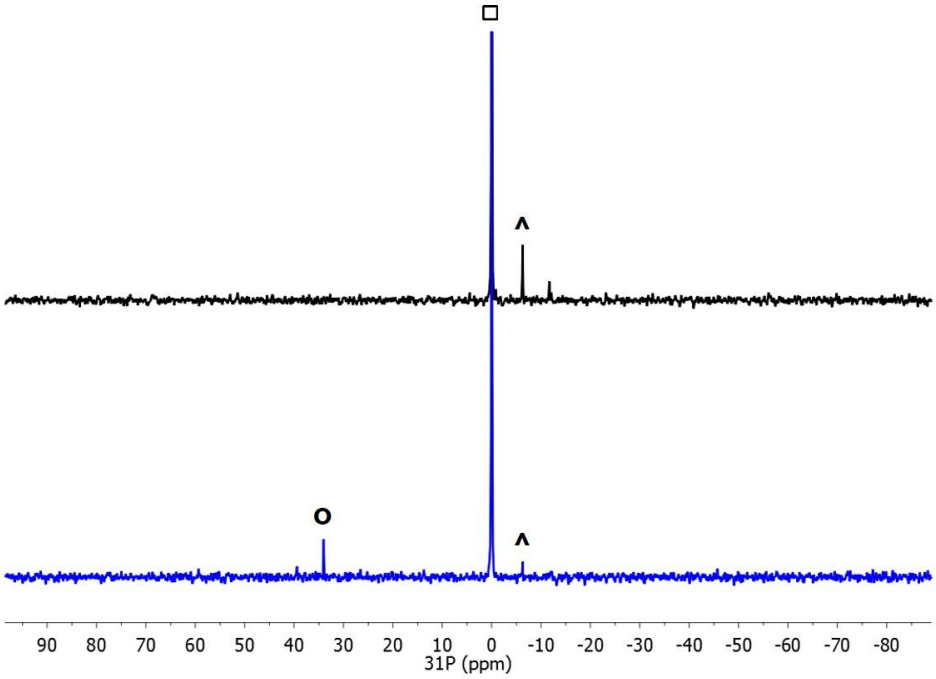

Fig. S7. $^{31}P\{^{1}H\}$ NMR spectra of $[HPt(dmpe)_2](PF_6)$ (top) and after addition 1 equivalent of protonated 1,8-diazabicyclo[5.4.0]undec-7-ene tetrafluoroborate (bottom). Where ^ denotes $[HPt(dmpe)_2]^+$, **o** denotes $[Pt(dmpe)_2]^{2+}$, and • denotes H_3PO_4 in capillary.

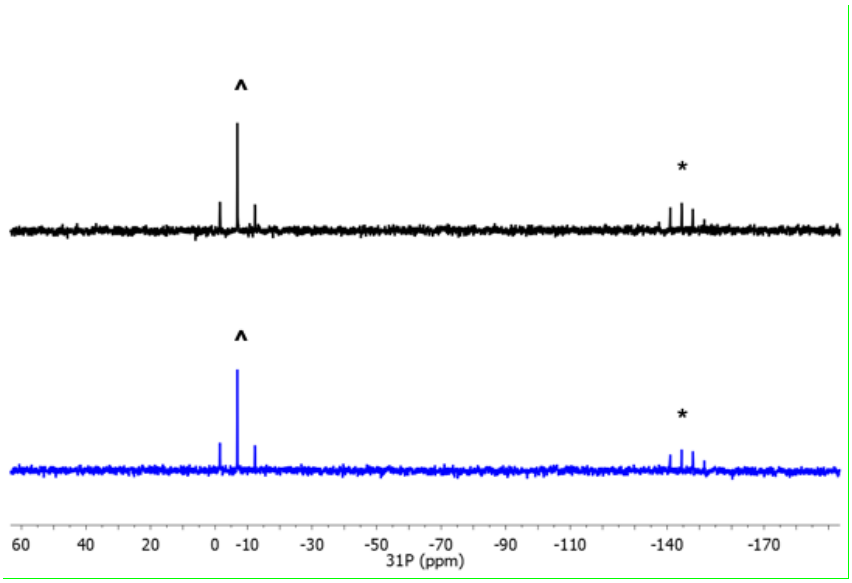

Fig S8. $^{31}P\{^{1}H\}$ NMR spectra of $[HPt(dmpe)_2](PF_6)$ (top) and after addition 1 equivalent of phenol (bottom). Where ^ denotes $[HPt(dmpe)_2]^+$ and * denotes PF_6 ion.

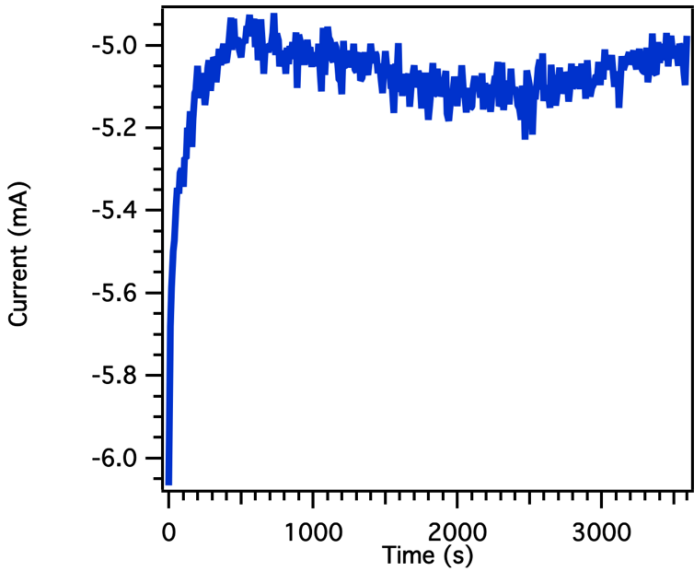

Fig. S9. Current vs. Time plot of 1 hour electrolysis at -2.4 V vs. $Fe(C_5H_5)_2^{+/0}$ of 1 mM $[Pt(dmpe)_2](PF_6)_2$, 10 mM phenol and 1 mM $FeCp_2$ with 0.1 M $TBAPF_6$ in CH_3CN; under CO_2 (run 1). Total charge passed: 18.2 C; 3.14 equivalents of charge with respect to **3**.

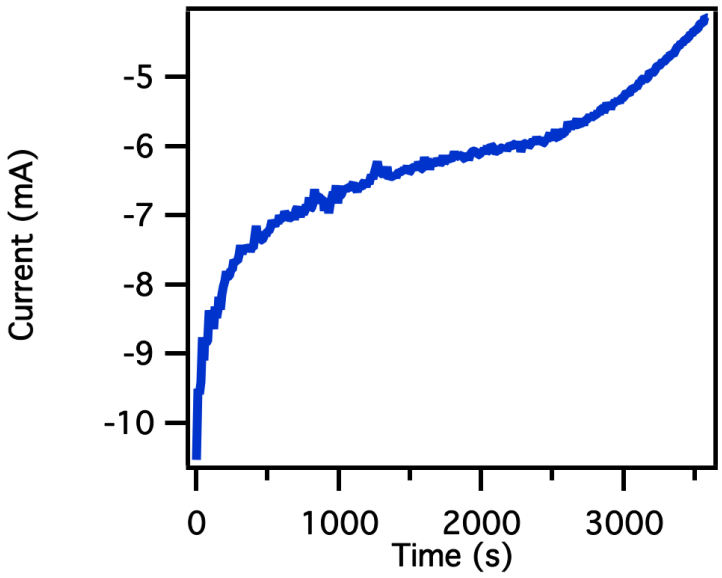

Fig. S10. Current vs. Time plot of 1 hour electrolysis at -2.3 V vs. $Fe(C_5H_5)_2^{+/0}$ of 1 mM $[Pt(dmpe)_2](PF_6)_2$, 10 mM phenol and 1 mM $FeCp_2$ with 0.1 M $TBAPF_6$ in CH_3CN; under CO_2 (run 2). Total charge passed: 22.4 C; 3.87 equivalents of charge passed with respect to **3**.

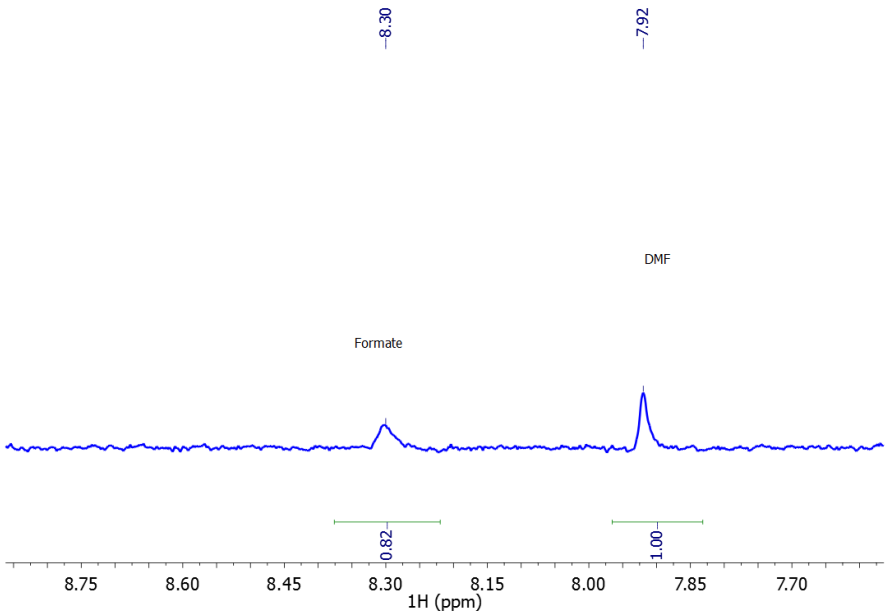

Fig. S11. ^{1}H NMR post electrolysis solution of run 1 with DMF standard (method A formate quantification). Run 1 electrolysis solution: 10 mM phenol and 1 mM $Fe(C_5H_5)_2$ with 0.1 M $TBAPF_6$ in CH_3CN; under CO_2.

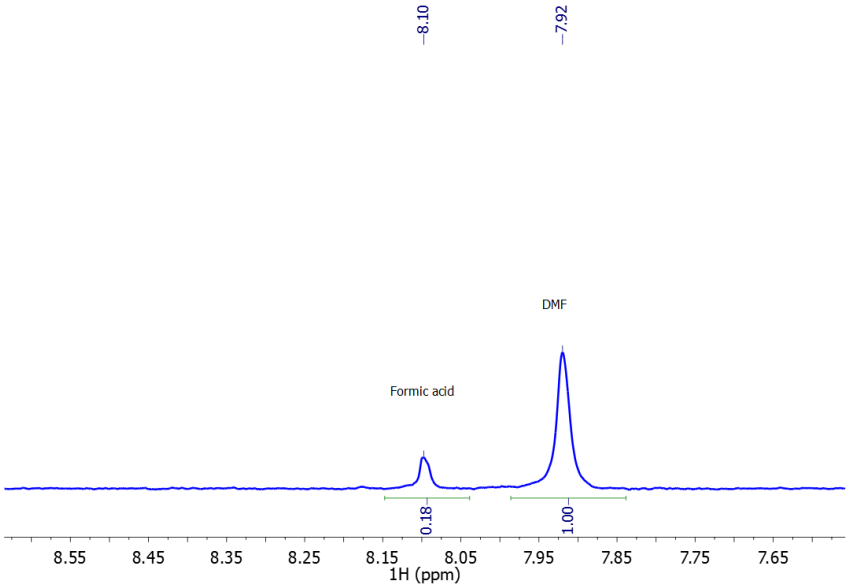

Fig. S12. ^{1}H NMR post electrolysis solution of run 1 with DMF standard following solution acidification (method B formic acid quantification). Run 2 electrolysis solution: 10 mM phenol and 1 mM $Fe(C_5H_5)_2$ with 0.1 M $TBAPF_6$ in CH_3CN; under CO_2.

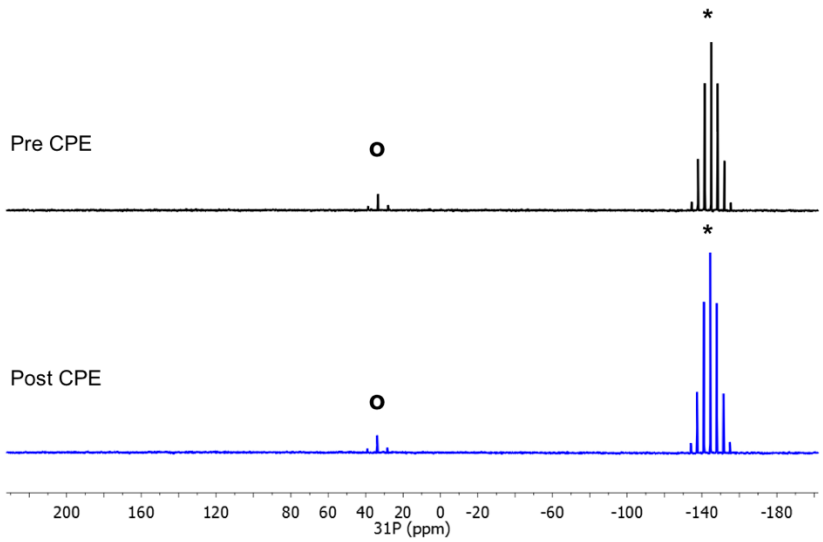

Fig. S13. $^{31}P\{^{1}H\}$ NMR spectra of pre- (top) and post- (bottom) electrolysis solution (run 1); where **o** denotes $[Pt(dmpe)_2]^{2+}$ and * denotes PF_6 ion. Run 1 electrolysis solution: 1 mM $[Pt(dmpe)_2](PF_6)_2$, 10 mM phenol, and 1 mM $Fe(C_5H_5)_2$ with 0.1 M $TBAPF_6$ in CH_3CN; under CO_2.

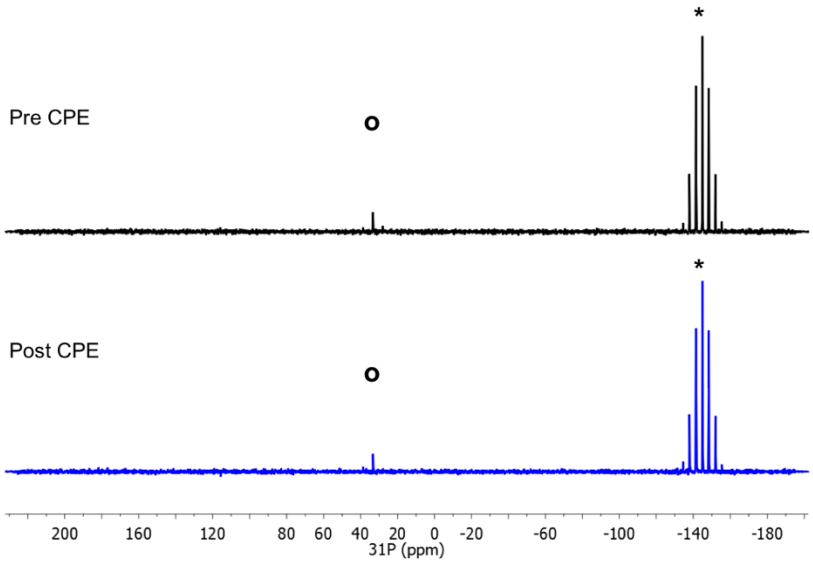

Fig. S14. $^{31}P\{^{1}H\}$ NMR spectra of pre- (top) and post- (bottom) electrolysis solution (run 2); where **o** denotes $[Pt(dmpe)_2]^{2+}$ and * denotes PF_6 ion. Run 2 electrolysis solution: 1 mM $[Pt(dmpe)_2](PF_6)_2$, 10 mM phenol, and 1 mM $Fe(C_5H_5)_2$ with 0.1 M $TBAPF_6$ in CH_3CN; under CO_2.

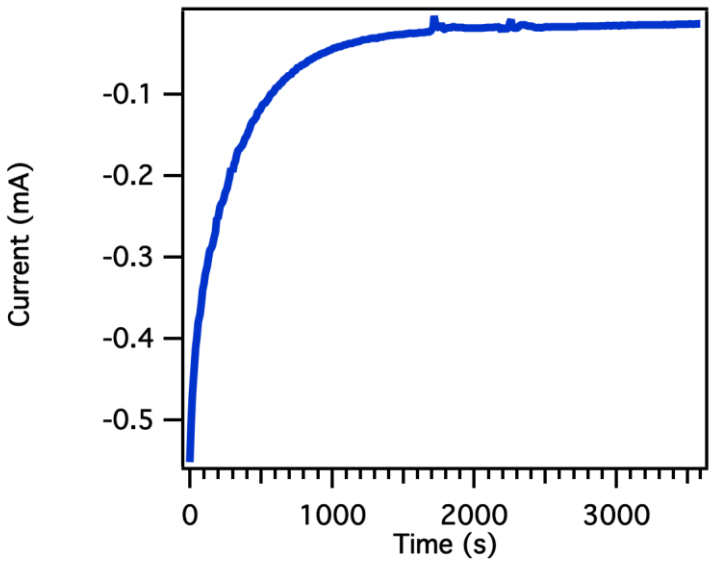

Fig. S15. Current vs. Time plot of 1 hour electrolysis at -2.3 V vs. $Fe(C_5H_5)_2^{+/0}$ of 10 mM phenol and 1 mM $Fe(C_5H_5)_2$ with 0.1 M $TBAPF_6$ in CH_3CN; under CO_2 without catalyst. Total charge passed: 0.215 C; 0.0371 equivalents of charge passed with respect to $Fe(C_5H_5)_2$.

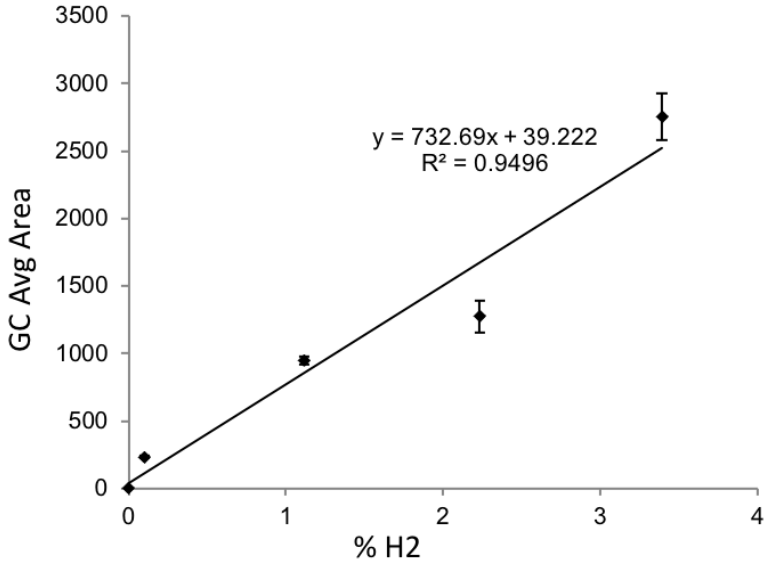

Fig. S16. GC calibration curve for H_2 with 1 hour mixing time in acetonitrile. Points show average peak area and error bars show the standard deviation across 6 measurements. Linear fit equations are shown on the graph.

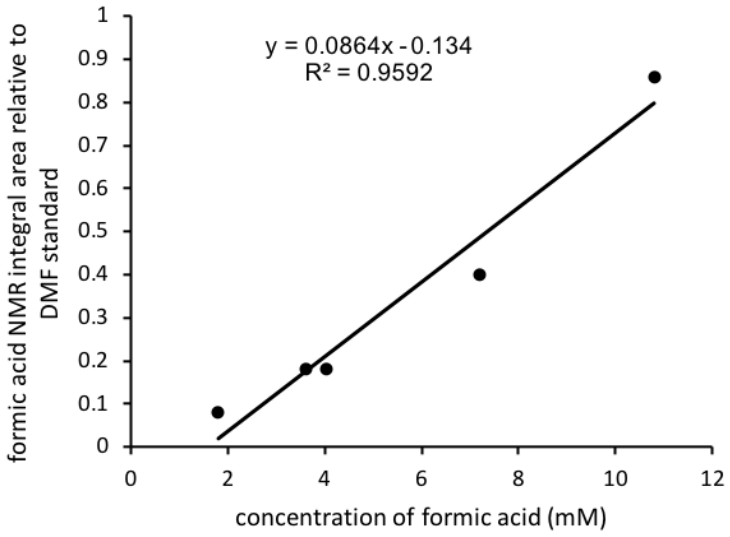

Fig. S17. ^{1}H NMR solvent suppression calibration curve for formic acid in acetonitrile. Points show peak area Linear fit equations are shown on the graph.

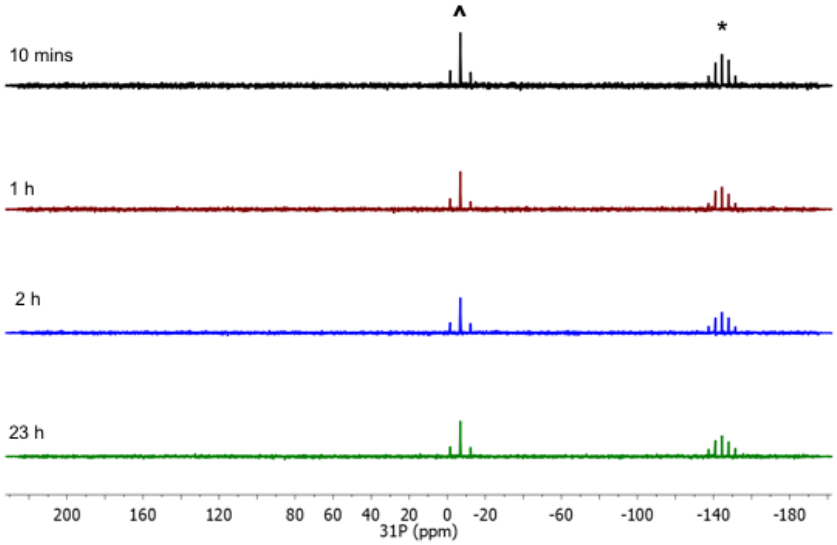

Fig. S18. $^{31}P\{^{1}H\}$ NMR spectra of $[HPt(dmpe)_2](PF_6)$ in solution over 23 hours. Where ^ denotes $[HPt(dmpe)_2]^+$ and * denotes PF_6 ion.

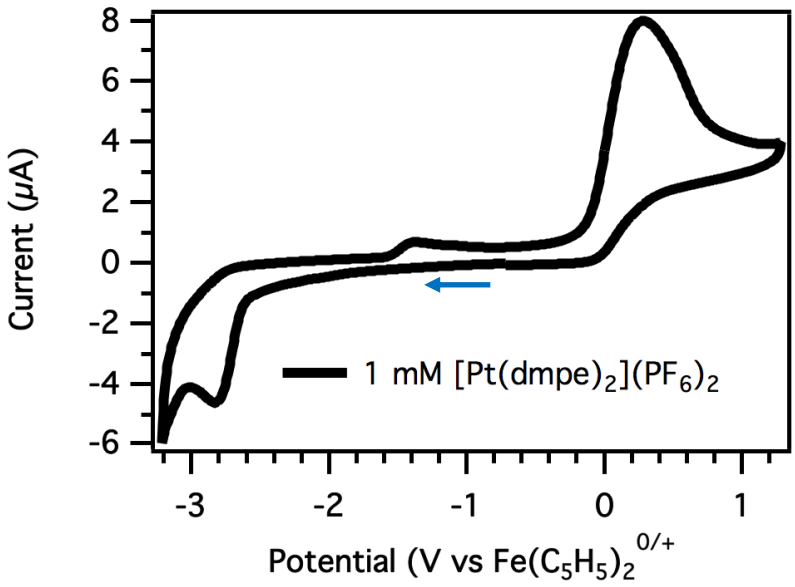

Fig. S19. Cyclic voltammetry of 1 mM [HPt(dmpe)$_2$](PF$_6$) (**2**) in 0.1 M TBAPF$_6$ in CH_3CN at 100 mV/s scan rate; under N_2.

References

1. Curtis, C. J.; Miedaner, A.; Ellis, W. W.; DuBois, D. L., Measurement of the Hydride Donor Abilities of [HM(diphosphine)2]+ Complexes (M = Ni, Pt) by Heterolytic Activation of Hydrogen. *J. Am. Chem. Soc.* **2002,** *124* (9), 1918-1925.
2. Berning, D. E.; Noll, B. C.; DuBois, D. L., Relative Hydride, Proton, and Hydrogen Atom Transfer Abilities of [HM(diphosphine)2]PF6 Complexes (M = Pt, Ni). *J. Am. Chem. Soc.* **1999,** *121* (49), 11432-11447.
3. Nicholson, R. S.; Shain, I., Theory of Stationary Electrode Polarography. Single Scan and Cyclic Methods Applied to Reversible, Irreversible, and Kinetic Systems. *Anal. Chem.* **1964,** *36* (4), 706-723.
4. Saveant, J. M.; Vianello, E., Potential-sweep chronoamperometry: Kinetic currents for first-order chemical reaction parallel to electron-transfer process (catalytic currents). *Electrochim. Acta* **1965,** *10* (9), 905-920.
5. Saveánt,J.-M. *Elements of Molecular and Biomolecular Electrochemistry*; John Wiley & Sons, Inc.: Hoboken, NJ, 2006.